Journal of Alloys and Compounds Communications 3 (2024) 100026

Contents lists available at ScienceDirect

Journal of Alloys and Compounds Communications

journal homepage: www.sciencedirect.com/journal/jacomc

Oxidation and compositional modulation in single phase C14 $Zr_{0.6}Ti_{0.4}Fe_1Cr_1$ alloy

Sakine Khajavi [a,b,*], Sabine Schlabach [c,d], Astrid Pundt [c], Jacques Huot [a]

[a] Hydrogen Research Institute, Université du Québec à Trois-Rivières, 3351 des Forges, Trois-Rivières G9A 5H7, Canada
[b] National Center for Electrochemistry and Environmental Technologies, 2263, Avenue du Collège, Shawinigan G9N 6V8, Canada
[c] Institute for Applied Materials (IAM), Karlsruhe Institute of Technology, Kaiserstraße 12, Karlsruhe D-76131, Germany
[d] Karlsruhe Nano Micro Facility (KNMFi), Karlsruhe Institute of Technology, Karlsruhe D-76131, Germany

ARTICLE INFO

Keywords:
Metal hydrides
AB_2 alloys microstructure
C14 crystal structure
EBSD
Heat-treatment
Rietveld refinement

ABSTRACT

This study investigates the effects of heat treatment on the crystal structure and hydrogen absorption behavior of the AB_2 type metal hydride $Zr_{0.6}Ti_{0.4}Fe_1Cr1$. The objective is to understand how 3- and 6-day heat treatments at 1000°C influence the alloy's microstructure and hydrogenation properties. Using electron microscopy, EBSD analysis, X-ray diffraction, and hydrogenation measurements, we found that the as-cast alloy exhibits rapid hydrogen absorption with significant compositional variations due to segregation during casting, confirmed by a single C14 Laves phase in XRD. Heat treatment slowed hydrogen absorption and reduced hydrogen capacity, with XRD indicating the structure remained primarily C14 Laves phase. However, SEM/EDS analysis showed substantial microstructural changes, including the emergence of new phases and segregation of Zr-rich phases, likely non-hydride forming, influenced by elevated oxygen content. These new phases probably contribute to the reduced hydrogen uptake capacity.

1. Introduction

Hydrogen as an energy vector is a vital component for the development of clean renewable energy systems [1]. Between different ways of hydrogen storage, metal hydrides are a good choice because of their high volumetric capacities and reasonable temperature of operation [2–5].

The Laves phase AB_2 alloys are one of the interesting metal hydrides for hydrogen storage. In Laves phase alloys, the atomic radius ratio r_A/r_B should be between 1.05 and 1.7 [6]. In metal hydrides, usually A is a hydride forming element and B is a non-hydride forming element but this is not a strict rule [7–9].

The Zr-based and Ti-based AB_2 alloys have different hydrogenation properties. High stability is a distinctive feature of Zr-based Laves phase alloys which lead to difficult desorption due to the low plateau pressure [1,9]. On the other hand, the equilibrium pressure in Ti-based Laves phase alloys is too high and exhibits high hysteresis [10–12]. Thus, substituting Zr for Ti on the A site may improve the hydrogen storage properties of this AB_2 alloy by combining the advantages of these two A site elements [13,14]. It has been shown that in $Ti_{1-x}Zr_xMn_1Cr_1$ and $Ti_{1-x}Sc_xMn_1Cr_1$ alloys, increasing x made the first hydrogenation easier and increased the capacity [13,15].

Iba and Akiba have demonstrated that $Zr_{0.5}Ti_{0.5}V_1Mn_1$ alloy crystallizes in a C14 matrix with body-centred cubic (bcc) colonies containing small α-ZrO_2 particles resulting from residual oxygen [16]. They also showed that the total hydrogen capacity is the sum of the individual phases capacities. Boettinger et al. have shown that solidification of the battery electrode material (Zr, Ti)(V, Cr, Mn, Ni)$_2$ alloys result in a microstructure characterized by a dendritic growth of the hexagonal C14 Laves phase, peritectic solidification of a cubic C15 Laves phase, and formation of a cubic B2 phase in the interdendritic regions [17]. Khajavi et al. demonstrated that the alloys of composition $(Zr_{0.5}Ti_{0.5})(Mn_{1-x}Fe_x)Cr_1$, where x = 0, 0.2, 0.4, has a Laves type hexagonal crystal structure (space group $P6_3/mmc$, strukturbericht notation C14). They also reported on a large variation in composition, discussed in the data treatment with two C14 phases with two different chemical compositions. They also emphasized that while all alloys may appear to comprise two C14 structures with similar lattice parameters and chemical compositions, when composition variation is minimal, fitting with only one phase is feasible. Thus, the concept of two coexisting C14 phases should not be taken too literally but rather as indicating significant compositional variation within the C14 phase [18,19].

* Corresponding author at: Hydrogen Research Institute, Université du Québec à Trois-Rivières, 3351 des Forges, Trois-Rivières G9A 5H7, Canada.
E-mail address: s.khajavi65@gmail.com (S. Khajavi).

https://doi.org/10.1016/j.jacomc.2024.100026
Received 18 June 2024; Received in revised form 10 August 2024; Accepted 20 August 2024
Available online 22 August 2024

In this paper we present the investigation of the $Zr_{0.6}Ti_{0.4}Fe_1Cr_1$ alloy microstructure before and after heat treatment for 3 and 6 days at 1000°C. First hydrogenation kinetics of these samples are also reported. The effect of heat treatment on the thermodynamics is better evaluated by measuring the enthalpy and entropy of hydrogenation/dehydrogenation. This paper mainly focuses on the kinetics of first hydrogenation. The thermodynamic parts will be the subject of another study.

2. Experimental method

All pure elements Fe (99.9 %), Ti (99.9 %), Zr (99.5 %), Mn (99.9 %) and Cr (99 %) were purchased from Alfa Aesar. The alloys were prepared by arc melting under 0.7 bars of argon. Each pellet was melted and turned over three times in order to get homogeneity. Heat treatment of the alloy was performed at 1000°C for 72 and 144 hours under a constant flow of argon. At the end of the heat treatment, the samples were returned to room temperature by simply turning off the furnace while keeping the argon flow. Primary microstructure and chemical analysis were performed using a Hitachi Su1510 scanning electron microscopy equipped with an EDS (energy-dispersive X-ray) apparatus from Oxford Instruments. Relative abundance of each phase evaluated from micrograph analysis using the software Image J. The crystal structure was determined by X-ray diffraction using a Bruker D8 Focus with Cu Kα radiation. Lattice parameters were evaluated from Rietveld's method, using Topas software [20].

Additional EDS and EBSD measurements were done at the Karlsruhe Nano Micro Facility ($KNMF_i$). The instrument used was a Zeiss Auriga 60 with EDAX/AMETEK EDS-detector Octane Super A and with EDAX/AMETEK EBSD-detector DIGI View V under 20 kV voltage.

Hydrogenation measurements were performed at room temperature under 20 bars of hydrogen on a homemade Sievert's apparatus using the volumetric method.

3. Result

3.1. Structure of arc-melted alloy

The X-ray diffraction pattern of alloy $Zr_{0.6}Ti_{0.4}Fe_1Cr_1$ in as-cast state is shown in Fig. 1A. This pattern presents a single C14 phase. The rising background with angle is due to the iron fluorescence associated with Cu Kα radiation. However, the electron backscattered micrograph of Fig. 1B shows bright and grey areas which indicates a variation in the chemical composition as it was already observed in our previous work [18,19]. For $(Zr_{0.5}Ti_{0.5})(Mn_{1-x}Fe_x)Cr_1$ alloys where x = 0, 0.2, 0.4, it was shown that the Laves phase has a range of chemical compositions which resulted in a distribution of lattice parameters and thus a broadening of the peaks [18].

A chemical analysis was performed on bright and grey spots and the results are shown on Table 1. The iron and chromium content (B site of C14 phase) are practically constant, but the titanium and zirconium concentrations are almost the exact opposite in the bright and grey regions.

The fact that the Zr+Ti abundance is constant is a confirmation that Zr and Ti are on the same site in the AB_2 C14 phase. The AB_2 binary compounds of these four elements all crystallize in Laves phases. The room temperature phase of $TiFe_2$ effectively crystallizes in the C14 phase. However, for $ZrFe_2$, $ZrCr_2$ and $TiCr_2$ the stable room temperature phase is instead the cubic C15 phase (space group *Fd-3m*) which is also a Laves phase. In the case of $ZrCr_2$ and $TiCr_2$ a high-temperature C14

Table 1
Chemical composition, in at%, in specific spots of $Zr_{0.6}Ti_{0.4}Fe_1Cr_1$ alloy.

Area	Ti	Zr	Fe	Cr
bright	12	27	31	30
grey	25	11	32	32

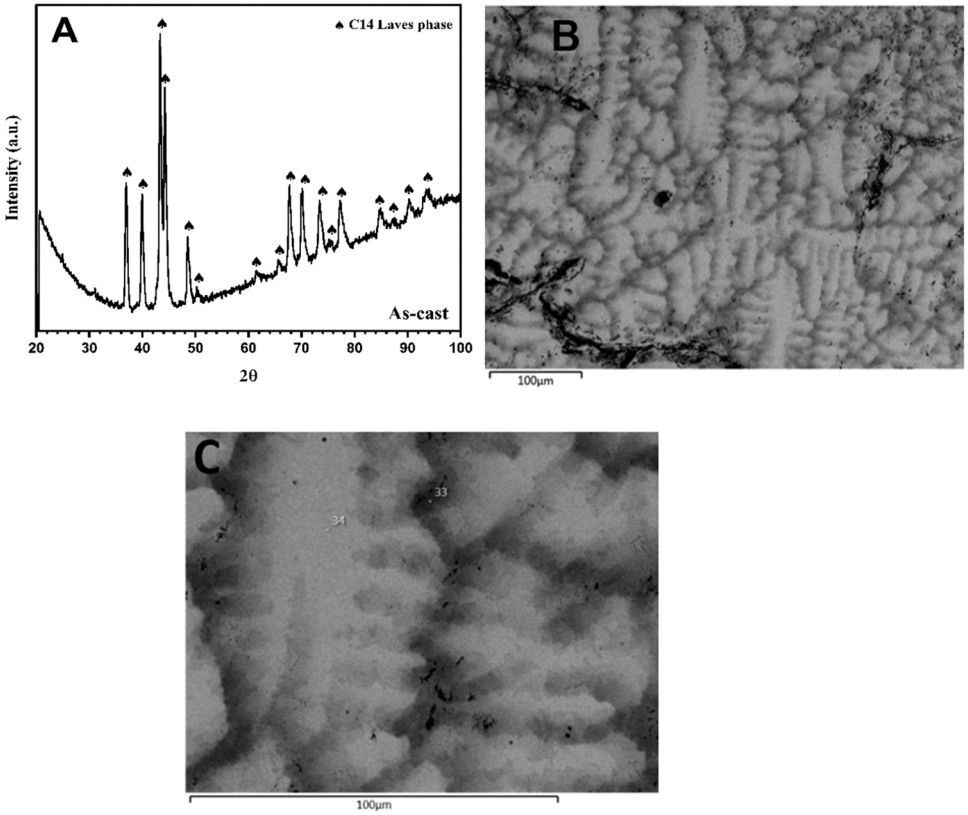

Fig. 1. As-cast $Zr_{0.6}Ti_{0.4}Fe_1Cr_1$ alloy. A: X-ray powder diffraction. B-C: Electron backscattered micrograph.

phase exists.

The reason why the phase adopted by the present alloy is C14 instead of C15 is probably due to the metastable nature of the sample because the cooling rate of arc melting is relatively high. For this reason, we have performed heat treatment on this alloy, in a similar way as was done in our previous investigation [18]. Heat treatment was performed at 1000°C under argon flow for a duration of 3 and 6 days.

Fig. 2 shows a SEM image of the microstructure of the as-cast alloy, performed on the curved and non-polished surface at KNMF$_i$. The measurements position is indicated by the blue arrow in the upper left image in Fig. 2. Visible are elongated structures with smaller structures in between. It should be noted that Fig. 2 shows a much smaller field of view compared to Fig. 1. The EDS elemental mapping and line scan reveal Zr-rich dendrites and Fe, Cr and Ti-rich interdendrite region. We note that the surface topography may slightly influence the detected absolute concentration values. The gray shade regions within the Zr-rich dendrites don't show chemical differences.

Fig. 3 shows further SEM images of the microstructure and EDS data of the as-cast $Zr_{0.6}Ti_{0.4}Fe_1Cr_1$ alloy, after surface polishing. The viewing direction of the investigated area in this figure is roughly 90° with respect to Fig. 2, as shown in the upper left image. In Fig. 3(B)-(E) dendrite rich and more globular like areas can be distinguished. The EDS performed at various points show very similar spectra but a slight change in the relative intensities of the peaks. The chemical composition of these points are given in Tables 2 and 3.

From Table 2 we see that the surface is heavily oxidized particularly for spots 1 and 2. Surface oxidation is expected by the alloy elements. There is also a large amount of carbon. This may be due to surface contamination. In Table 3 we present the abundances rescaled by taking into account only Ti, Zr, Cr and Fe. This will make the comparison with the nominal values easier.

Spot 1 has a high oxygen content and is probably some complex oxide. For the other spots, the chromium and iron abundances are very close to the nominal values. They vary by less than 10 % of the nominal values. However, the situation is completely different for the zirconium and titanium abundances. Here, the variation is much bigger, about 35 % each for titanium and zirconium. In a previous investigation, we have shown that there is a variation of composition within the C14 phase of $Ti_{0.5}Zr_{0.5}(Mn_{1-x}Fe_x)Cr_1$ where x = 0, 0.2 and 0.4[18]. Here, we see that this variation is mainly on the A atoms (Zr and Ti) and not so much on the B atoms (Fe and Cr).

An inverse pole figure map taken on the polished surface is shown in Fig. 4 along with an elemental mapping. Most of these regions could be indexed to a C14 Laves phase. We also can see that the grains in this area are roughly globular and of the order of a few 10 μm. The intragranular region is zirconium-rich and titanium poor.

Such compositional inhomogeneity is known to appear during the casting process. They originate from segregation occurring during cooling from the melt through two-phase fields in the phase diagram when the diffusivity of the elemental species in the final phase is insufficient. They can be removed by annealing in the single phase field. As the phase diagram of the four-component system is not known, experimental approaches have to be used.

3.2. 3 days Heat-Treated

To affect the compositional inhomogeneity, and also, to test the stability of the detected C14 phase, the as-cast alloy was heat treated at 1000°C under argon flow for 3 days. For the investigation the sample has been polished using the same viewing direction as in Fig. 3. Fig. 5 shows the SEM micrograph taken at UQTR and Table 4 shows the chemical composition of three spots in this image. After 3 days of heat treatment, the sample still shows intensity variations in the SEM BSE images of the polished sample. EDS reveal local chemical variations deviating from the nominal composition.

Fig. 6 (A) shows a backscattered electron image at low magnification. Regions with different grey shades could be seen.

Fig. 6 (B) shows a subsection of Fig. 6 (A) and Table 5 gives the element abundance at specific spots.

As for the as-cast alloy, the surface is heavily oxidized. Oxidation is expected by the alloy elements. One spot also featured aluminum. This may be due to contamination from an initial polishing before the diamond lapping film polishing. A better comparison with nominal values is possible by excluding these contaminants as shown in Table 6.

Spot 1 shows almost a Zr:Ti=1 composition. As Zr and Ti are completely miscible in the binary system, this is reasonable to imagine that such a phase may be formed during heat treatment. Spot 2 is titanium-rich and is probably a titanium precipitate. Spot 3 has a composition that is relatively (Zr-Ti)(Cr-Fe)$_2$. Therefore, the local crystal structure is most likely C14. Spot 4 is mainly made of Cr and Fe. In the binary Cr-Fe phase diagram, there is a tetragonal phase CrFe that is stable between 460°C and about 830°C. Here, this phase may be further stabilized by the small amount of Zr and Ti, possibly also by some O. Finally, spot 5 is mainly a mixture of Zr, Cr and Fe. The elemental mapping in Fig. 6 (D) shows areas mainly enriched in Zr, Cr and Ti are overlapping in some areas as well as Cr and Fe in some others, whereas areas enriched in Ti show typically no Fe. By EBSD, the C14 Laves phase could not be detected unambiguously. Possibly, α-Ti-rich phase, $FeCr_2O_3$ and other phases have been formed in the multielemental system.

Three days annealing of the alloy at 1000°C is thus not sufficient for reaching a homogeneous elemental distribution. Contrary to the assumption, the inhomogeneity is even enhanced. This can originate

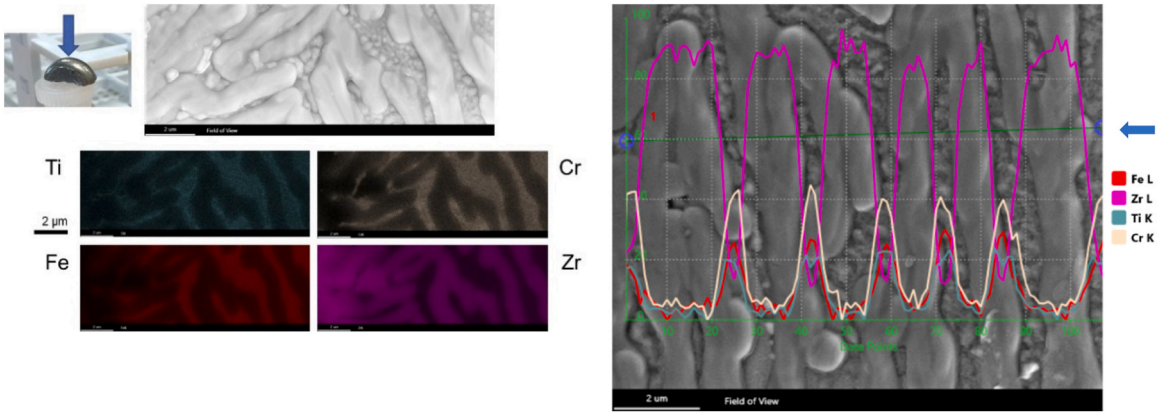

Fig. 2. SEM micrographs on the microstructure and EDS analysis for as-cast $Zr_{0.6}Ti_{0.4}Fe_1Cr_1$ alloy, on the non-polished surface. The blue arrow in the upper left image indicates the analysis position. Elemental mapping and line scan (in at%) are slightly affected by surface topography. The position of the line scan is marked by a green line (blue arrow).

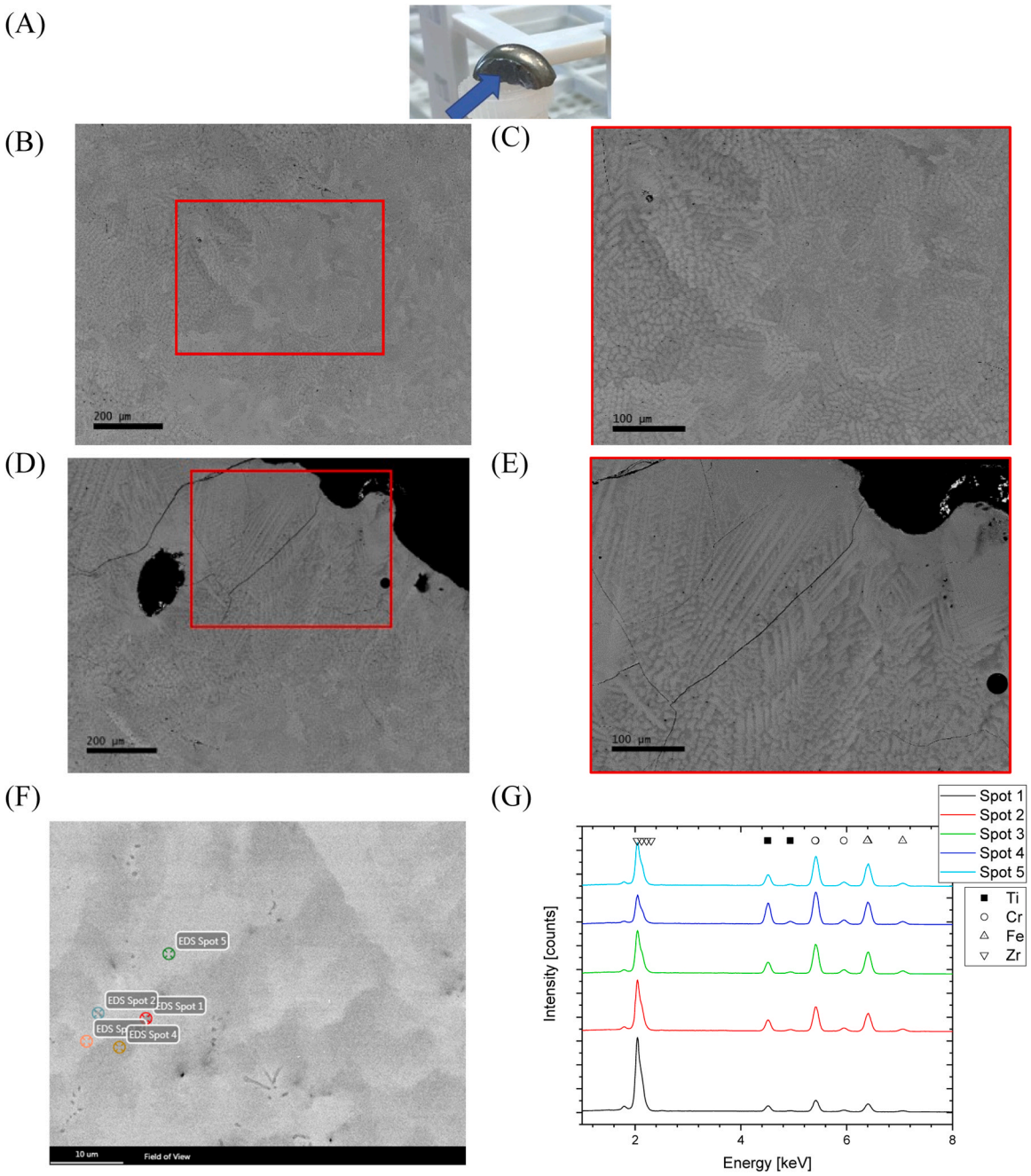

Fig. 3. SEM micrographs on the microstructure and EDS data of the as-cast $Zr_{0.6}Ti_{0.4}Fe_1Cr_1$ alloy after polishing. The investigated area is marked by an arrow in (A). Specific surfaces are shown in (B, C) and (C, D). Micrograph F indicates the specific points for EDS analysis which spectra are shown in G.

Table 2
Elements abundances of the as-cast $Zr_{0.6}Ti_{0.4}Fe_1Cr_1$ alloy. All values are in at%. Spot # relates to Fig. 3.

Spot #	Ti	Zr	Fe	Cr	C	O
1	3.2	18.5	6.8	7.8	20.2	43.5
2	6.3	13.9	16.2	17.0	20.9	25.6
3	7.1	13.5	22.65	22.9	27.4	6.2
4	12.6	9.0	23.1	24.9	24.0	6.4
5	6.6	13.7	22.0	22.5	28.9	6.2

Table 3
Normalized abundances of Ti, Zr, Cr and Fe in the as-cast $Zr_{0.6}Ti_{0.4}Fe_1Cr_1$ alloy. All values are in at%. Spot # relates to Fig. 3.

Spot #	Ti	Zr	Fe	Cr
1	8.8	51.0	18.7	21.5
2	17.4	26.0	30.3	31.8
3	10.7	20.4	34.2	34.6
4	18.1	12.9	33.2	35.8
5	10.2	21.1	34.0	34.7
Nominal	13.3	20.0	33.3	33.3

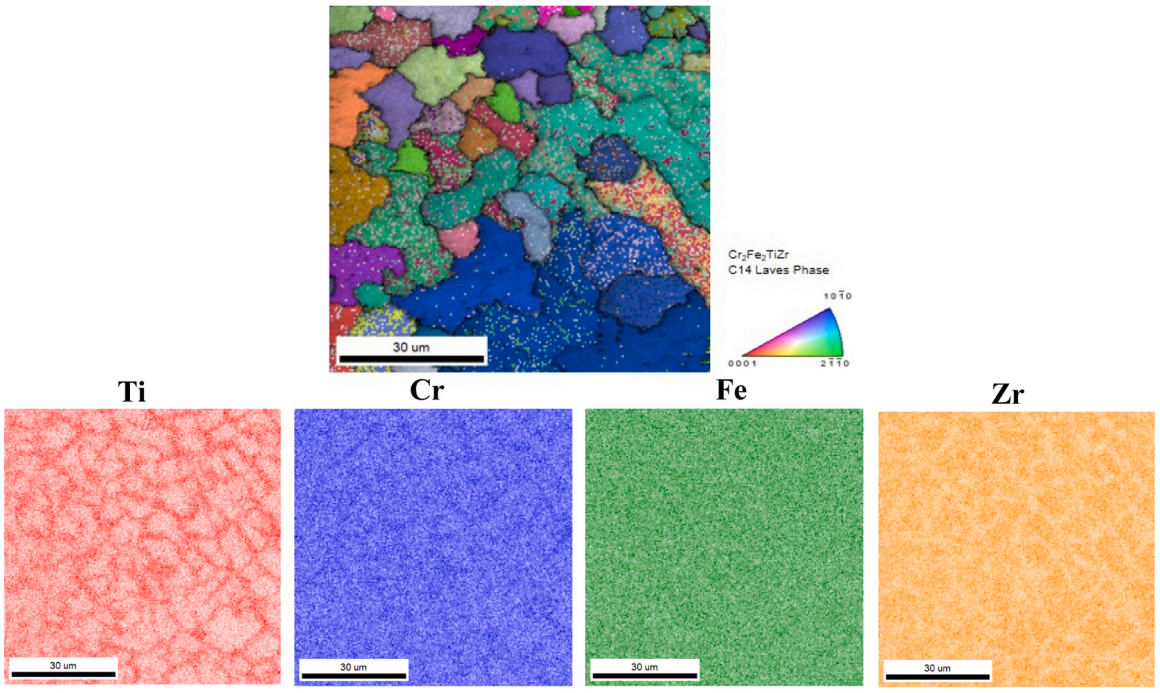

Fig. 4. Inverse pole figure map and element mapping of as-cast $Zr_{0.6}Ti_{0.4}Fe_1Cr_1$ alloy. Viewing direction is identical to that in Fig. 3.

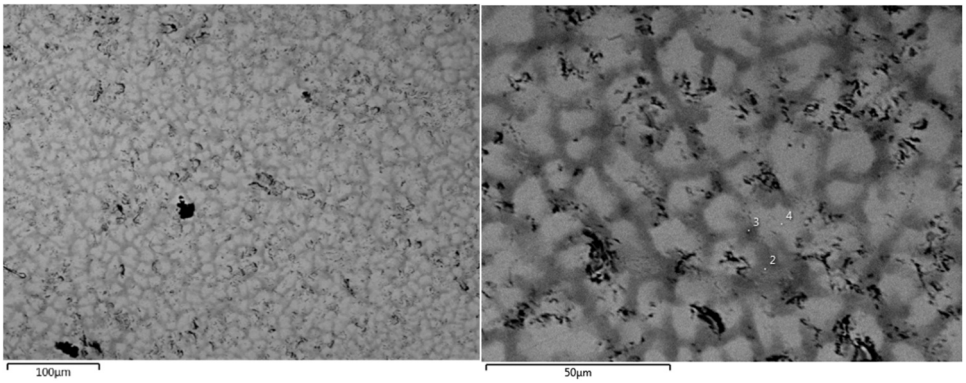

Fig. 5. Electron backscattered micrograph of 3-day heat-treated $Zr_{0.6}Ti_{0.4}Fe_1Cr_1$ alloy.

Table 4
Chemical composition, in at%, obtained by EDS in specific spots of 3 days heat-treated $Zr_{0.6}Ti_{0.4}Fe_1Cr_1$ alloy.

Area	Ti	Zr	Fe	Cr
bright	9.2	24.5	33.6	32.7
Light grey	17.5	17.4	32.4	32.7
Dark grey	16.5	12.0	28.7	42.8
Nominal	13.3	20.0	33.3	33.3

from insufficient diffusivity, from local melting of concentration regions with low melting temperature or from new phases containing oxygen.

3.3. 6 days Heat-Treated

A longer heat treatment of 6 days at 1000°C under argon flow was performed on the as-cast $Zr_{0.6}Ti_{0.4}Fe_1Cr_1$ alloy. For the investigation, the sample has been polished using the same viewing direction as in Fig. 2. Fig. 7 shows the SEM micrograph taken at UQTR and Table 7 shows the chemical composition in different spots of this image.

Compared with Table 4, the composition in selected points is less homogeneous than for the 3 days heat treated sample. This, again, is an indication of some phase segregation or reaction with oxygen and carbon.

Fig. 8 (A) to (C) shows the microstructure of this sample taken at KNMF$_i$. The chemical composition as measured by EDS of the specific spots (Fig. 8 (B) and (C)) are given in Table 8. For the 6 days heat treatment, the EDS spectra from one spot to another are quite different and the amount of C and O is still very high.

Table 9 shows the normalized element abundance without C, O and Al.

The elemental mapping is shown in Fig. 8 (D). From this figure a separation of the elements is even more distinct than in the 3 days heat treated sample. The titanium and zirconium are totally decoupled from each other and from the other elements. On the other hand, iron and chromium seems to be coupled together. Possibly, α-Ti-rich phase, $FeCr_2O_3$ and other phases have been formed.

Furthermore, analyzing Fig. 9 provides insight into the enrichment of a specific phase resulting from heat treatment. Upon closer examination of these images, a noticeable decline in sample homogeneity is evident following heat treatment, diverging from the anticipated outcome. This suggest that the as-cast state is relatively homogeneous but is

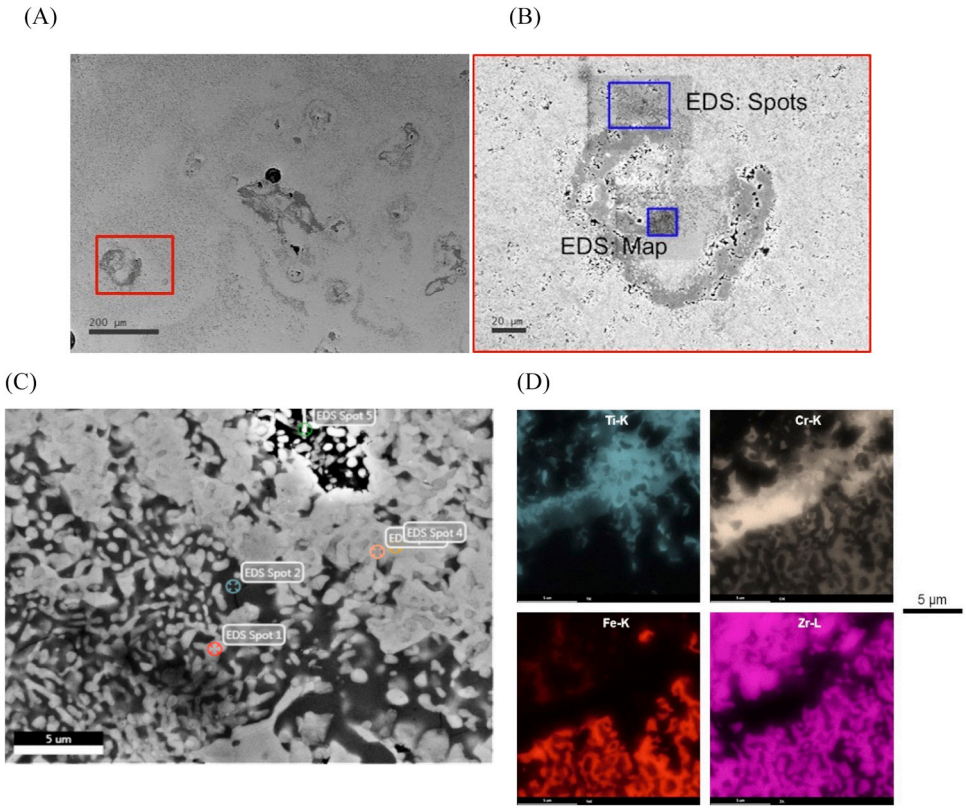

Fig. 6. Low magnification SEM BSE image (A) of $Zr_{0.6}Ti_{0.4}Fe_1Cr_1$ alloy after 3 days of heat treatment at 1000°C together with a higher magnification of a selected area (B). Areas for EDS spot analysis (C) and for elemental mapping (D) are marked with blue rectangles in (B).

Table 5
Elements abundances at specific spots of Fig. 6C in $Zr_{0.6}Ti_{0.4}Fe_1Cr_1$ alloy after 3 days of heat treatment at 1000°C. All values are in at%.

Spot #	Ti	Zr	Fe	Cr	Al	C	O
1	10.9	10.0	0.8	0.7	0.0	31.1	46.6
2	24.8	2.8	2.5	2.7	0.2	20.3	26.8
3	3.7	9.3	8.8	8.1	0.0	37.9	32.9
4	1.3	4.4	22.1	18.6	0.0	39.2	14.5
5	1.6	13.4	3.8	3.7	8.0	26.4	43.2

Table 6
Normalized abundances of Zr, Ti, Cr and Fe at specific spots in $Zr_{0.6}Ti_{0.4}Fe_1Cr_1$ alloy after 3 days of heat treatment at 1000°C. All values are in at%.

Spot #	Ti	Zr	Fe	Cr
1	48.7	44.6	3.6	3.1
2	75.6	8.5	7.6	8.2
3	12.3	31.1	29.4	27.1
4	2.2	9.5	47.6	40.0
5	7.1	59.6	16.9	16.4
Nominal	13.3	20.0	33.3	33.3

metastable. Upon heat treatment the metastable phase revert to more stable phases. Additionally, a distinct Zr-rich specific phase is clearly observed, likely indicating the presence of Zr or alpha ZrO_2, as observed by Khajavi et al. [18].

3.4. Crystal structure

The X-ray powder diffraction of as-cast, 3 days and 6 days heat-treated $Zr_{0.6}Ti_{0.4}Fe_1Cr_1$ alloy are shown in Fig. 10. The annealing was also performed to test the stability of the detected C14 phase. In Fig. 9, the diffraction pattern of all three alloys show similar diffraction peaks.

A Rietveld refinement was performed on each pattern and the results are shown in Table 10.

Table 10 indicates that there are only small variation of parameters from one sample to the other. According to the Rietveld refinement, only one phase is present, namely the Laves phase hexagonal structure of space group $P6_3/mmc$ and structure type $MgZn_2$. This is a Frank-Kasper structure with Strukturbericht designation C14. It should be stressed here that, as also found in a previous investigation on a different alloy [19], the Rietveld refinement parameter 'microstrain' is not a micro-strain but instead reflects the chemical variation within the C14 phase, as detectd in the EDS measurements.The residue of the Rietveld refinement did not indicate the presence of any other phases beside the C14 phase. This may seem contradictory to the SEM results presented in the preceding sections where chemical compositions suggested the presence of additional phases. However, in the SEM investigation, we focused on small inclusions. They might be in total too small to be detectable in the X-ray powder diffraction. As these small inclusions may act as nucleation points for the formation of the hydride they are worth investigating. The SEM investigation also showed that the surface was heavily oxidized. Oxide phases commonly lead to many diffraction peaks of low intensity. These phases may be hidden in the background of the XRD pattern. Specifically, the presence of newly formed zirconium-rich precipitates is evident in the SEM results. However, peaks associated with Zr precipitates are not detected in the XRD pattern.

Thus, X-ray powder diffraction of as-cast, 3 days and 6 days heat-treated $Zr_{0.6}Ti_{0.4}Fe_1Cr_1$ alloy did verify a certain stability of the C14 Laves phase. However, this phase is not stable in the presence of oxygen and partly decomposes in other phases during heat treatment. Local concentrations that hint on a CrFe phase were found, too.

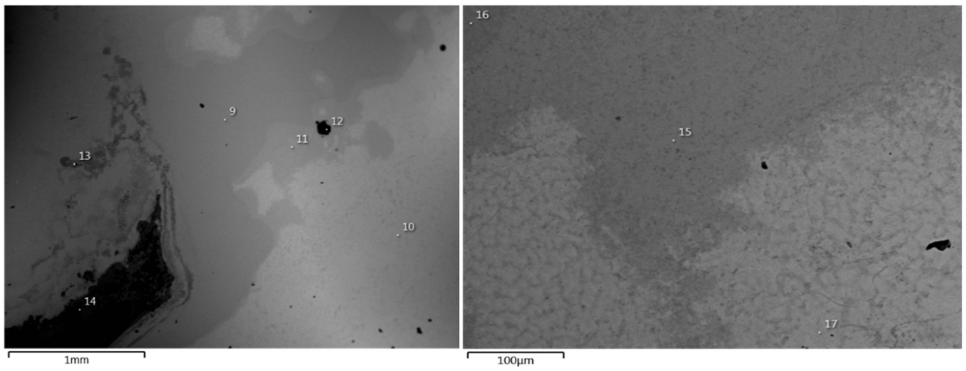

Fig. 7. Electron backscattered micrograph of 6 days heat-treated $Zr_{0.6}Ti_{0.4}Fe_1Cr_1$ alloy.

Table 7
Elements abundances at specific spots (Fig. 7) in $Zr_{0.6}Ti_{0.4}Fe_1Cr_1$ alloy after 6 days of heat treatment at 1000°C. All values are in at%.

Spot #	Ti	Zr	Fe	Cr
9	1.2	25.3	36.2	37.3
10	13.9	20.5	33.4	32.2
11	12.6	17.2	40.1	30.1
12	3.9	28.4	34.0	33.6
13	46.7	17.7	18.1	17.5
14	46.6	2.2	2.0	49.2
15	9.3	21.6	42.5	26.7
16	1.2	16.4	41.7	40.8
17	14.7	17.7	36.3	31.3
27	76.3	22.0	0.9	0.7
28	95.1	0.9	2.0	2.0
Nominal	13.3	20.0	33.3	33.3

3.5. Hydrogenation

The first hydrogenation curves of as-cast and heat-treated $Zr_{0.6}Ti_{0.4}Fe_1Cr_1$ alloy are shown in Fig. 11, under 2 MPa hydrogen pressure and at room temperature. Before hydrogenation, the alloys were manually crushed in a glove box to enhance the surface-to-volume ratio. The particle size was on average less than 500 µm. This technique is conventionally applied in our group. The hydrogen absorption kinetics of the as-cast alloy is fast and shows no incubation time. It reaches

Table 8
Elements abundances at specific spots (Fig. 8) in $Zr_{0.6}Ti_{0.4}Fe_1Cr_1$ alloy after 6 days of heat treatment at 1000°C. All values are in at%.

Spot #	Ti	Zr	Fe	Cr	Al	C	O
2	18.6	6.6	3.0	3.1	0.3	35.2	33.2
3	1.7	4.3	19.7	17.7	0.0	41.6	15.0
4	1.3	5.4	19.2	17.1	0.0	42.5	14.5
5	5.9	7.8	11.6	11.8	0.1	32.3	30.5

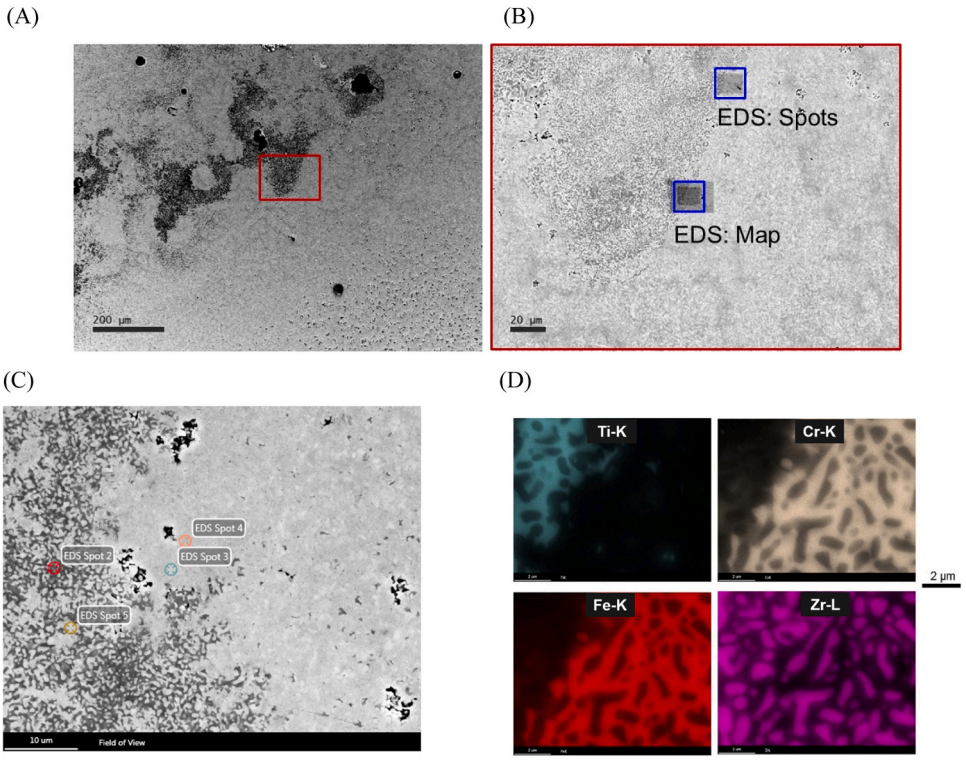

Fig. 8. (A) Low magnification backscatter electron image of $Zr_{0.6}Ti_{0.4}Fe_1Cr_1$ alloy after 6 days of heat treatment at 1000°C. (B) higher magnification of a selected area. (C) Marked positions of EDS spot analysis (results are in Tables 8 and 9). (D) elemental mapping.

Table 9
Normalized abundances of Ti, Zr, Cr and Fe at specific spots (Fig. 8) in $Zr_{0.6}Ti_{0.4}Fe_1Cr_1$ alloy after 6 days of heat treatment at 1000°C. All values are in at%.

Spot #	Ti	Zr	Cr	Fe
2	59.4	21.1	9.9	9.6
3	3.9	9.9	40.8	45.4
4	3.0	12.6	39.8	44.7
5	15.9	21.0	31.8	51.8
Nominal	13.3	20.0	33.3	33.3

full capacity in about 300 sec. This kinetics is substantially faster than what was reported for the $Ti_{0.5}Zr_{0.5}Mn_1Cr_1$ alloy [18]. The kinetics of the heat-treated alloys are slower than their as-cast counterparts and they show a loss of capacity. Close inspection of the kinetics shows that the intrinsic kinetics (slope at mid-capacity) is very similar for the three samples. The main difference being an incubation time present for the 3 and 6 days heat treatments. This may be due to a surface barrier that is reduced by the presence of hydrogen. Alternatively, the lack of incubation time for the as-cast sample may indicate a metastable nature of the C14 phase that facilate hydrogen penetration. Since heat treatments potentially could stabilize alloys and convert metastable phases to more stable ones, we propose this hypothesis. However, metastability of the C14 phase is not confirmed from the present investigation and more experiments are needed to test this hypothesis.

As it is obvious in Fig. 11, the loss of capacity is more important for the alloy annelaed for 6 days than the one annealed for 3 days. Thus, the heat treatment has a detrimental effect on both the capacity and kinetics. This detrimental effect may be related to oxidation during heat treatment and the presence of other phases, as indicated by SEM investigations. For instance, non-hydride phases like ZrO_2, which do not absorb hydrogen, were observed. However, the 20 % loss in capacity from the as-cast to the 6-day heat-treated alloys cannot solely be attributed to the presence of a minor phase practically undetectable by XRD. This suggests another underlying reason. In the as-cast alloy, a hydrogen capacity of 1.6 wt% was recorded which correspond to a hydrogen over metal ration (H/M) of 1. But theoretically, a H/M-ratio of 1.2 is possible as reported by Pourarian et al. for $ZnMn_2H_{3.6}$ [21]. For the present alloy, a specific A site of the C14 structure has a 60 % probablity of being a Zr atom and 40 % of being a Ti atom. In the same way, for the two B sites the probablility of a specific site is 50 % for Fe and 50 % for Cr. This means that there are a variety of atomic surroundings for the H atoms, each one having a different energy. This will most likely lead to a sloping plateau. We also saw from the SEM investigation that there is a range of chemical compositions for the C14 phase. Therefore, the probability of having a specific atom on a specific site also varies. This will contribute to the variation of the energy of interstitial sites. Upon heat treatment the compositional range is shortened thus having an effect of the slope and position of the plateau. This may be the reason for the reduction of capacity upon heat treatment. The real explanation will come from PCT measurements. This will be the subject of a future paper.

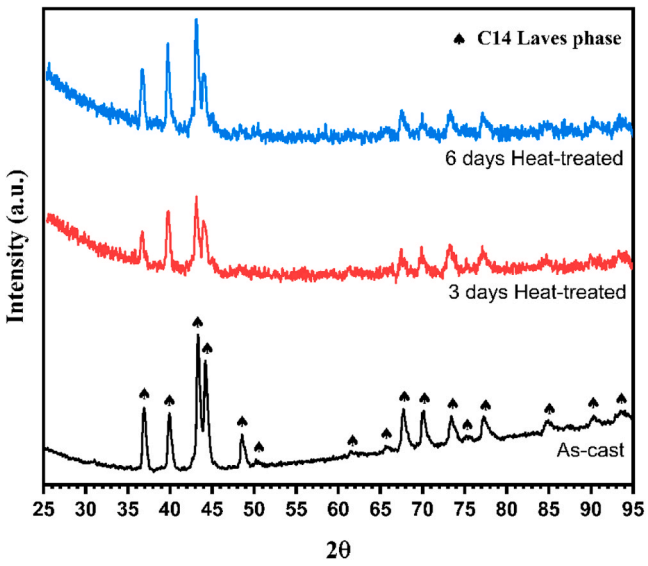

Fig. 10. XRD pattern of as-cast, 3 days HT and 6 days HT of $Zr_{0.6}Ti_{0.4}Fe_1Cr_1$ alloy.

4. Summary

The crystal structure and the first hydrogen absorption behaviour of the AB_2 alloy $Zr_{0.6}Ti_{0.4}Fe_1Cr_1$ has been investigated in the as-cast state and after heat treatment by electron microscopy and X-ray powder diffraction. The SEM/EDS studies demonstrated a strong compositional variation in the C14 phase of the as-cast alloy. This compositional variation within one phase may occur after casting when the elemental

Table 10
Parameters of the C14 phase determined by Rietveld refinements of $Zr_{0.6}Ti_{0.4}Fe_1Cr_1$ alloy in the as-cast, 3 days and 6 days heat treatment. The error on the last significant digit is shown in parentheses.

Sample	a Å	c Å	Unit cell volume Å^3	Crystallite size nm	Microstrain %
As-cast	4.961(1)	8.145(2)	173.9(1)	37(5)	0.21(1)
3 days HT	4.966(2)	8.148(4)	174.0(2)	68(4)	0.24(2)
6 days HT	4.959(2)	8.136(4)	173.39(2)	43(12)	0.21(1)

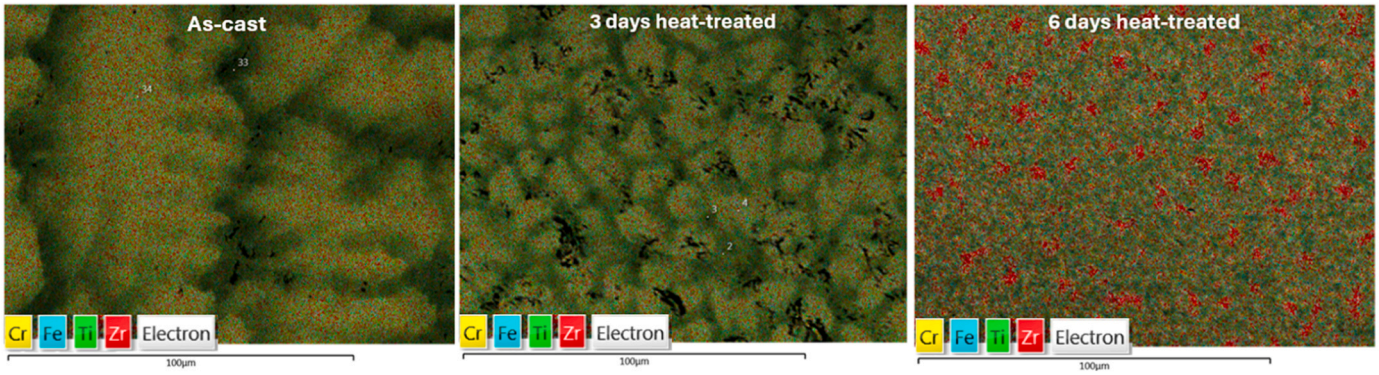

Fig. 9. The impact of heat treatment on the elemental distribution of $Zr_{0.6}Ti_{0.4}Fe_1Cr_1$ alloy components. An enrichment of Zr-rich specific phase is detected after 6 days of heat treatment.

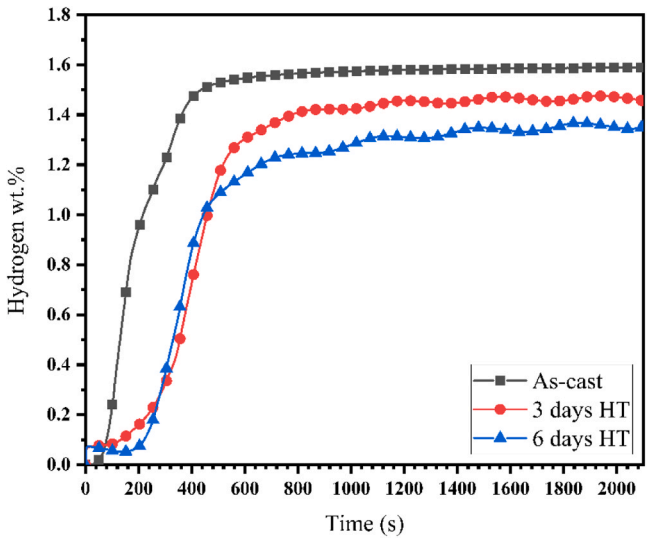

Fig. 11. Activation curves of as cast, 3 days heat-treated and 6 days heat-treated $Zr_{0.6}Ti_{0.4}Fe_1Cr_1$ alloy.

diffusivity in the final phase is small. This as cast alloy with the concentration modulation shows the fastest hydrogen uptake, also when compared to other similar alloys.

Annealing was performed to homogenize the alloy and to test for C14 phase stability. After heat treatment at 1000°C, X-ray powder diffraction reveal that the crystal structure of the Laves phase did not change. Thus, XRD measurements confirm C14 phase beeing present throughout the whole experimental series. Upon annealing, the compositional variations measured by EDS even increased. A part of the C14 phase was found to decompose into other phases among which some of them contain oxygen.

CRediT authorship contribution statement

Sakine Khajavi: Conceptualization, Investigation, Methodology, Visualization, Formal analysis, Writing - Original Draft, Writing - Review & Editing, Validation, Corresponding author. **Sabine Schlabach:** Investigation, Formal analysis, Resources, Writing - Review & Editing. **Astrid Pundt:** Investigation, Formal analysis, Resources, Writing - Review & Editing. **Jacques Huot:** Supervision, Investigation, Conceptualization, Methodology, Formal analysis, Resources, Writing - Review & Editing.

Declaration of Competing Interest

The authors declare that they have no known competing financial interests or personal relationships that could have appeared to influence the work reported in this paper.

Data availability

All data are available in article.

Acknowledgements

AP likes to acknowledge stimulating discussions with Dr. A. Kauffmann, IAM-WK, KIT.

References

[1] T.B. Zhang, et al., Hydrogen absorption properties of Zr(V1−xFex)2 intermetallic compounds,", Int. J. Hydrog. Energy vol. 37 (3) (2012) 2328–2335.
[2] P. Chen, M. Zhu, Recent progress in hydrogen storage, Mater. Today vol. 11 (12) (2008) 36–43. /12/01/ 2008.
[3] S. Studer, S. Stucki, J.D. Speight, Hydrogen as a Fuel. Hydrogen as a Future Energy Carrier, Wiley-VCH Verlag GmbH & Co. KGaA, 2008, pp. 23–69.
[4] A. Züttel, Introduction. Hydrogen as a Future Energy Carrier, Wiley-VCH Verlag GmbH & Co. KGaA, 2008, pp. 1–6.
[5] J.R. Anstrom, 17 - Hydrogen as a fuel in transportation. Advances in Hydrogen Production, Storage and Distribution, Woodhead Publishing, 2014, pp. 499–524.
[6] F. Stein, M. Palm, G. Sauthoff, Structure and stability of Laves phases. Part I. Critical assessment of factors controlling Laves phase stability, Intermetallics vol. 12 (7) (2004) 713–720. /07/01/ 2004.
[7] A. Jain, S. Agarwal, D. Vyas, P. Jain, I.P. Jain, Correlation between the milling time and hydrogen storage properties of ZrCrFe ternary alloy, Int. J. Hydrog. Energy vol. 35 (18) (2010) 9910–9915.
[8] E.D. Koultoukis, S.S. Makridis, E. Pavlidou, P. de Rango, A.K. Stubos, Investigation of ZrFe 2 -type materials for metal hydride hydrogen compressor systems by substituting Fe with Cr or V, Int. J. Hydrog. Energy vol. 39 (36) (2014) 21380–21385.
[9] J. Hidalgo-Jimenez, J.M. Cubero-Sesin, K. Edalati, S. Khajavi, J. Huot, Effect of high-pressure torsion on first hydrogenation of Laves phase Ti0.5Zr0.5(Mn1-xFex)Cr1 (x = 0, 0.2 and 0.4) high entropy alloys, J. Alloy. Compd. 969 (2023) 172243.
[10] T.A. Zotov, R.B. Sivov, E.A. Movlaev, S.V. Mitrokhin, V.N. Verbetsky, IMC hydrides with high hydrogen dissociation pressure, J. Alloy. Compd. vol. 509 (2011) S839–S843.
[11] S.V. Mitrokhin, V.N. Verbetsky, Ti-based laves phase hydrides with high dissociation pressures (no. Supplement C), J. Alloy. Compd. vol. 253-254 (1997) 201–202.
[12] M. Au, F. Pourarian, S.G. Sankar, W.E. Wallace, L. Zhang, TiMn2-based alloys as high hydrogen storage materials, Mater. Sci. Eng.: B vol. 33 (2) (1995) 53–57. /09/01/ 1995.
[13] X. Guo, E. Wu, Thermodynamics of hydrogenation for Ti1−xZrxMnCr Laves phase alloys, J. Alloy. Compd. vol. 455 (1) (2008) 191–196. /05/08/ 2008.
[14] X. Guo, E. Wu, S. Wang, Hydrogen storage properties of Laves phase Ti1−xZrx (Mn0.5Cr0.5)2 alloys, Rare Met. vol. 25 (6) (2006) 218–223.
[15] W. Li, E. Wu, P. Ma, K. Sun, D. Chen, Hydrogen storage properties of Ti1−xScxMnCr Laves phase alloys,", Int. J. Energy Res. vol. 37 (7) (2013) 686–697.
[16] H. Iba, E. Akiba, The relation between microstructure and hydrogen absorbing property in Laves phase-solid solution multiphase alloys, J. Alloy. Compd. vol. 231 (1) (1995) 508–512. /12/15/ 1995.
[17] D.E.N.W.J. Boettinger, K. Wang, L.A. Bendersky, C. Chiu, U.R. Kattner, K. Young, B. Chao, Examination of Multiphase (Zr,Ti)(V,Cr,Mn,Ni)2 Ni-MH Electrode Alloys: Part I. Dendritic Solidification Structure, Metall. Mater. Trans. A vol. 41 (8) (2010) 2033–2047.
[18] S. Khajavi, M. Rajabi, J. Huot, Crystal structure of as-cast and heat-treated Ti0.5Zr0.5(Mn1-xFex)Cr1, x=0, 0.2, 0.4, J. Alloy. Compd. (2018). /07/11/ 2018.
[19] S. Khajavi, M. Rajabi, J. Huot, Effect of cold rolling and ball milling on first hydrogenation of Ti0.5Zr0.5 (Mn1-xFex)Cr1, x = 0, 0.2, 0.4, J. Alloy. Compd. vol. 775 (2019) 912–920. /02/15/ 2019.
[20] A.X.S.T.V. Bruker, "General profile and structure analysis software for powder diffraction data," in *InUser's Manual, ed.* Karlsruhe, Germany, 2005.
[21] F. Pourarian, V.K. Sinha, W.E. Wallace, H.K. Smith, Kinetics and thermodynamics of ZrMn2-based hydrides, J. Less Common Met. 88 (1982) 451–458.